

MTMR4, a phosphoinositide-specific 3'-phosphatase, regulates TFEB activity and the endocytic and autophagic pathways.

メタデータ	言語: eng 出版者: 公開日: 2019-04-25 キーワード (Ja): キーワード (En): 作成者: メールアドレス: 所属:
URL	https://doi.org/10.24517/00053882

This work is licensed under a Creative Commons Attribution-NonCommercial-ShareAlike 3.0 International License.



MTMR4, a phosphoinositide-specific 3'-phosphatase, regulates TFEB activity and the endocytic and autophagic pathways

Hoa Quynh Pham¹, Kazuaki Yoshioka¹, Hiromi Mohri¹, Hiroki Nakata², Sho Aki¹, Kazuhiro Ishimaru¹, Noriko Takuwa^{1,3} and Yoh Takuwa¹

¹Department of Physiology, Kanazawa University School of Medicine, Kanazawa,

²Department of Histology and Cell Biology, Kanazawa University School of

Medicine, Kanazawa, ³Department of Health and Medical Science, Ishikawa

Prefectural Nursing University, Kahoku, Japan

Short title: MTMR4 regulation of endocytic pathways

Keywords: MTMR4, phosphatidylinositol 3-phosphate, endosome, lysosome, autophagosome, autophagy, membrane traffic, TFEB

All correspondence should be addressed to ytakuwa@med.kanazawa-u.ac.jp (Yoh Takuwa, M.D., Ph.D.).

ABSTRACT

Phosphatidylinositol 3-phosphate (PI(3)P) is the predominant phosphoinositide species in early endosomes and autophagosomes, in which PI(3)P dictates traffic of these organelles. Phosphoinositide levels are tightly regulated by lipid-kinases and –phosphatases; however, a phosphatase that converts PI(3)P back to phosphatidylinositol in the endosomal and autophagosomal compartments is not fully understood. We investigated the subcellular distribution and functions of myotubularin–related protein-4 (MTMR4), which is distinct among other MTMRs in that it possesses a PI(3)P–binding FYVE domain, in lung alveolar epithelium–derived A549 cells. MTMR4 was localized mainly in late endosomes and autophagosomes. MTMR4 knockdown markedly suppressed the motility, fusion and fission of PI(3)P–enriched structures, resulting in decreases in late endosomes, autophagosomes and lysosomes, and enlargement of PI(3)P–enriched early and late endosomes. In amino acid– and serum–starved cells, MTMR4 knockdown decreased both autophagosomes and autolysosomes, and markedly increased PI(3)P–containing autophagosomes and late endosomes, suggesting that the fusion with lysosomes of autophagosomes and late endosomes might be impaired. Notably, MTMR4 knockdown inhibited the nuclear translocation of starvation-stress responsive transcription factor-EB (TFEB) with reduced expression of lysosome–related genes in starved cells. These findings indicate that MTMR4 is essential for the integrity of endocytic and autophagic pathways.

1 INTRODUCTION

The endocytic pathway has multiple functions including degradation and recycling of macromolecules and signaling to the cytosol and nucleus, thus playing an essential role in cell homeostasis. It consists of a series of endosomes; early endosomes (EEs), recycling endosomes (REs), late endosomes (LEs) and lysosomes (LYs). In the endocytic pathway, EEs mature to become LEs and REs. LEs subsequently either fuse with LYs or mature further to become LYs (Huotari et al., 2011).

The autophagic pathway allows the orderly degradation and recycling of cellular components. Targeted cytoplasmic constituents are isolated from the rest of the cell within a double-membraned vesicle known as an autophagosome (AP), which eventually fuses with LYs and the contents are degraded and recycled (Komatsu & Ichimura, 2010; Mizushima et al., 2011; Carlsson et al., 2015).

Maturation and trafficking of endosomes and the process of autophagy are regulated coordinately by Rab GTPases and phosphoinositides (Armi et al., 2013; Balla, 2013; Li et al., 2013; Shen, et al., 2013; Wallroth et al., 2018).

Phosphatidylinositol 3-phosphate (PI(3)P) is the predominant phosphoinositide species in EEs, APs and in the internal vesicles of LE/multivesicular bodies (MVBs). PI(3)P recruits various effector proteins containing FYVE, PX and PH motifs (Schink et al., 2013). For example, EEA1, which is recruited to EEs through the PI(3)P-binding FYVE domain, cooperates with Rab5 to regulate early endosomal fusion (Fratti et al., 2001; Mu et al., 1995). PI(3)P is gradually metabolized along with the maturation of EEs toward LE, and is negligible in lysosomes (Huotari et al., 2011; Marat et al., 2016; Ketal, et al., 2016).

A large set of phosphoinositide-specific metabolizing enzymes have been identified. The myotubularin-related protein (MTMR) family of 3'-specific

phosphoinositide phosphatases can convert PI(3)P back to phosphatidylinositol (PI) (Hnia et al., 2012; Billcliff et al. 2014). Only nine of sixteen MTMR family members seem to have catalytic activities. Among the MTMRs, MTMR4 and the structurally related MTMR3 are catalytically active phosphatases, characterized by the presence of a PH-GRAM (pleckstrin homology, glucosyltransferase, Rab-like GTPase activator and myotubularin) domain and a FYVE domain. The unique presence of a PI(3)P-binding FYVE domain in MTMR4 raises the possibility that this protein may interact with endosomes (Lorenzo et al., 2005). Previous studies reported that MTMR4 is distributed mainly in the perinuclear vesicles, which include EEs, REs and LEs (Plant et al., 2009; Naughtin et al., 2010; Teo et al., 2016; St-Denis et al., 2016). However, the subcellular localization of MTMR4 is not fully understood. Moreover, several MTMRs have been implicated in autophagy (Vergne et al., 2009; Noda et al., 2010; Taguchi-Atarashi et al., 2010; Vergne et al., 2010; Zou et al., 2012; Al-Qusairi et al., 2013; Liu et al., 2014; Hao et al., 2016) and lysosomal storage disorder-related human diseases. MTM1 has been shown to be mutated in congenital X-linked centronuclear or myotubular myopathy (XLCNM) (Kioschis et al., 1996), while MTMR2 and MTMR13 have been shown to be mutated in Charcot-Marie-Tooth (CMT) neuropathy (Azzedine et al., 2003). MTMR4 has thus far not been linked to human diseases. However, we have recently found that genetic disruption of MTMR4 results in perinatal lethality due to pulmonary developmental defects in mice (Yoshioka K. et al., unpublished observations), suggesting an indispensable role of this MTMR isoform in mammalian development and homeostasis.

Here, we show in human pulmonary alveolar type II epithelium-derived cells that MTMR4 is localized mainly in LEs and APs to downregulate PI(3)P level in these organelles. MTMR4 knockdown profoundly impairs endosomal motility and its

maturation toward LEs and LYs, the formation of APs and autolysosomes (ALYs), and activation of the transcription factor TFEB, which is the master transcriptional regulator for the gene expression of lysosomal proteins. Thus, these data indicate that MTMR4 plays an essential role in the regulation of endocytic and autophagic pathways.

2 RESULTS

2.1 MTMR4 localizes mainly to LEs and APs in A549 cells

Lung tissues comprise several different types of cells including epithelial cells, vascular cells and fibroblasts. Among several human and mouse cells examined, human pulmonary alveolar type II epithelium-derived A549 cells expressed MTMR4 protein most abundantly (Fig. 1a). Besides A549 cells, HeLa cervical carcinoma cells expressed a high level of MTMR4 protein (Fig. 1a). HEK293T cells, mouse embryonic fibroblasts (MEF) and mouse lung endothelial cells (MLEC) expressed lower levels of MTMR4, whereas the other cells did not express readily detectable levels of MTMR4. We focused on A549 for studying the role of MTMR4.

Transfection of A549 cells with MTMR4-specific siRNA reduced the expression of MTMR4 protein by approximately 80% compared with control siRNA (Fig. 1b).

MTMR4 knockdown did not affect the expression of phosphatidylinositol 3-kinase class II α (PI3K-C2 α) or MTMR3, the latter of which is the closest in amino acid sequences to MTMR4 among the 16 MTMR family members in humans. In anti-MTMR4-immunostaining of A549 cells, MTMR4 knockdown reduced the punctate anti-MTMR4 signals (Fig. 1c).

We investigated the intracellular localization of MTMR4 by expressing enhanced green fluorescent protein (GFP)-tagged MTMR4 (GFP-MTMR4) and fluorescent probes (mRFP-2xFYVE for PI(3)P and mCherry-2xML1N for PI(3,5)P₂) to detect PI(3)P and PI(3,5)P₂, respectively, in combination with immunofluorescent staining and organelle-specific dye staining. The 2xML1N has been regarded as a PI(3,5)P₂-specific probe (Li et al., 2013), however, a recent study (Hammond et al., 2017) questioned the specificity of the 2xML1N. The punctate signals of GFP-MTMR4 overlapped well with the LE- and LY-specific dye LysoTracker in A549 cells (Fig.

1d *upper*). A substantial portion of GFP-MTMR4–positive (+) vesicles were enriched in PI(3,5)P₂, whereas only a small portion of GFP-MTMR4⁺ vesicles were enriched in PI(3)P (Fig. 1d middle and bottom). A part of GFP-MTMR4⁺ vesicles were positive for the LE markers Rab7 and CD63 (LAMP3) or the AP/autolysosome (ALY) marker LC3B (Fig. 1e). In contrast, GFP-MTMR4⁺ vesicles were barely positive for the LY marker LAMP1, the lamellar body (LB) marker ABCA3, the EE marker EEA1, and the RE marker Rab11. Thus, GFP-MTMR4 was localized largely in LEs and APs. We also determined the localization of endogenous MTMR4 by using anti-MTMR4 immunostaining. Endogenous MTMR4 was colocalized most prominently with Rab7-positive LEs and much less with LC3-positive ALs/ALYs (Fig. S1), which was quite similar to the results obtained with GFP-MTMR4 (Fig. 1e).

2.2 MTMR4 knockdown enlarges PI(3)P–enriched EEs and LEs, and decreases the numbers of APs and LYs

MTMR4 has been reported mainly to hydrolyze PI(3)P like other MTMR members (Hnia et al., 2012; Billcliff et al. 2014), although several members of the myotubularin family have also been implicated in the hydrolysis of PI(3,5)P₂ (Teo et al., 2016). We compared the size of PI(3)P– and PI(3,5)P₂–enriched vesicles in control and MTMR4–depleted cells expressing either mRFP-2xFYVE or mCherry-2xML1N. Histogram analysis of the size distribution revealed that the size of PI(3)P–enriched vesicles in MTMR4–depleted cells was greater compared with control cells (Fig. 2a). In contrast, there was no difference in the size of PI(3,5)P₂–enriched vesicles between control and MTMR4–depleted cells (Fig. 2b). Time-lapse live-cell imaging demonstrated that the motility, fusion and fission of PI(3)P–enriched but not

PI(3,5)P₂-enriched vesicles in MTMR4-depleted cells were impaired compared with control cells (Videos S1 & S2, and Fig. S2).

Immunostaining of mRFP-FYVE-stably expressing cells with anti-cell organelle-specific marker antibodies showed that PI(3)P was distributed widely in EEA1⁺ EEs (Fig. 2c) and only partly in Rab7⁺ LEs, LC3B⁺ APs and LAMP1⁺ LYs (Fig. 2d, e & f) in control cells. MTMR4 knockdown enlarged the EEA1⁺ PI(3)P-enriched endosomes (Fig. 2c). MTMR4 knockdown also induced the appearance of large Rab7⁺ LEs (Fig. 2d). MTMR4 knockdown reduced the numbers of Rab7⁺ LEs, LC3B⁺ AP and LAMP1⁺ LY (Fig. 2d, e & f). In contrast, MTMR4 knockdown increased the number of pro-surfactant protein C (proSPC)⁺ LB, which was also observed with electron microscopy (Fig. S3 a & b). In MTMR4-depleted cells, the add-back of the siRNA-resistant form of GFP-MTMR4 (GFP-R4'), but not only GFP, rescued the knockdown phenotype of enlarged PI(3)P-enriched endosomes (Fig. S4). In contrast, the expression of the siRNA-resistant, catalytically inactive mutant GFP-MTMR4(C407S) (GFP-R4(C407S)') failed to do so. In control cells, the expression of GFP-R4(C407S)' did not induce the MTMR4-knockdown phenotype.

Thus, MTMR4 knockdown greatly increased the endosomal PI(3)P level and reduced the LY number, suggesting that it arrested endosomes at an intermediate stage, blocking trafficking and/or maturation of endosomes toward LY.

2.3 MTMR4 knockdown reduces APs and ALYs and induces PI(3)P accumulation in APs and LEs upon starvation

A549 cells transfected with the mRFP-GFP-LC3B expression vector were incubated in complete growth medium (fed) or Hank's balanced salt solution without serum and amino acids (starved) for 4 h (Fig. 3a & b). The mRFP-GFP-LC3B fusion protein

associates with the membrane of AP, and after fusion of AP with LY, GFP fluorescence but not mRFP fluorescence of mRFP-GFP-LC3B is lost within the acidic environment of ALYs (Kimura et al., 2007). In the fed-condition, MTMR4 knockdown reduced the numbers of mRFP⁺ GFP⁺ APs (yellow) and mRFP⁺ ALYs (red) (Fig. 3a). Starvation tended to increase APs in control cells, and MTMR4 knockdown reduced the numbers of both APs and ALYs in starved cells (Fig. 3b). Electron microscopic observation also showed that starvation increased APs and ALYs whereas MTMR4 knockdown suppressed the starvation-induced increases in APs and ALYs (Fig. 3c).

We examined the impact of MTMR4 knockdown on starvation-induced changes in cellular PI(3)P level. Starvation by itself did not alter PI(3)P⁺ puncta in control cells, and MTMR4 knockdown in starved cells induced marked enrichment of PI(3)P in LCB3⁺ puncta (Fig. 4a). Starvation also increased PI(3)P-enriched Rab7⁺ LEs in control siRNA-transfected cells (Fig. 4b). MTMR4 knockdown by itself increased PI(3)P-enriched Rab7⁺ LEs in fed cells. MTMR4 knockdown-induced PI(3)P accumulation in Rab7⁺ puncta was more marked in starved cells, suggesting that starvation induced an increase in PI(3)P-enriched LEs and/or related structures including amphisomes. Overall, these data indicate that MTMR4 regulates cellular PI(3)P level in the autophagic pathway as well as the endosomal pathway.

2.4 MTMR4 knockdown impairs starvation-induced TFEB nuclear translocation and lysosome biogenesis

Because we found that MTMR4 knockdown reduced LYs and inhibited the starvation-induced increase in ALYs (Fig. 2f, and Fig. 3a & b), we speculated that MTMR4 might be necessary for lysosome biogenesis. Therefore, we determined the

activation or nuclear translocation of TFEB, the master transcription factor controlling lysosome biogenesis. In fed cells transfected with the GFP-tagged TFEB (GFP-TFEB) expression plasmid, GFP-TFEB was diffusely distributed in the cytoplasmic compartment. Starvation induced massive nuclear translocation of GFP-TFEB in control cells (Fig. 5a & b). In contrast, in MTMR4-depleted cells, nuclear translocation of GFP-TFEB did not occur (Fig. 5a & b). In cells in which MTMR4-related MTM1 was depleted, GFP-TFEB was translocated into the nucleus under the starved condition. We also determined nuclear translocation of endogenous TFEB with anti-TFEB immunostaining. Like the case of GFP-TFEB fluorescence observations, starvation induced nuclear translocation of endogenous TFEB in control and MTM1-depleted cells, but not in MTMR4-depleted cells (Fig. 5c & d).

Consistent with its inhibitory effect on TFEB nuclear translocation, MTMR4 knockdown attenuated the expression of TFEB target genes including the genes of H⁺-dependent ATPases, TRPML channel and cathepsins under the starved and fed conditions (Fig. 5e). We quantified the fluorescence intensity of cells stained with the pH-sensitive, LE- and LY-specific fluorescent dye LysoTracker by flow cytometry (Fig. 5f). MTMR4 knockdown substantially attenuated LysoTracker fluorescence, suggesting that the luminal pH of LysoTracker-containing organelles might not be low enough in MTMR4-depleted cells, likely through the low expression of H⁺-dependent ATPases. We determined lysosomal degradation of uptaken FITC-dextran. After 1 h uptake of FITC-dextran, the cells were washed and monitored for FITC-dextran remaining in cells for 4 h. The FITC-dextran within the cells gradually decreased and reached less than 30% of the initial level in control cells. MTMR4 knockdown attenuated a reduction of intracellular FITC-dextran, suggesting impaired degradation in MTMR4-depleted cells (Fig. 5g). These observations suggest that

MTMR4 is engaged in maintenance of lysosomal integrity through the mechanisms involving the regulation of TFEB activation.

2.5 MTMR4 knockdown alters phosphorylation status and subcellular localization of TFEB

The nuclear translocation of TFEB is regulated by its phosphorylation: the dephosphorylated form of TFEB translocates into the nucleus to stimulate transcription whereas the phosphorylated form stays outside the nucleus (Settembre et al., 2011). In MTMR4-depleted fed cells, the amount of dephosphorylated TFEB was similar to that in control cells (Fig. 6a). Nevertheless, the nuclear translocation of TFEB was inhibited in MTMR4-depleted cells (Fig. 5a & b). In MTMR4-depleted fed cells, the amount of phosphorylated TFEB was substantially greater (Fig. 6a & b) and the ratio of dephosphorylated TFEB/total TFEB was lower in MTMR4-depleted cells (Fig. 6b) compared with control cells. In fed cells, the addition of the lysosomotropic agent chloroquine, which impairs lysosomal function to stimulate lysosomal biogenesis, markedly increased the dephosphorylated form of TFEB with a reduction in phosphorylated TFEB, as reported previously (Settembre et al., 2012; Rocznik-Ferguson et al., 2012), showing the validity of our assay. When control cells were starved, the amount of dephosphorylated TFEB increased and, therefore, the ratio of dephosphorylated TFEB/total TFEB rose (Fig. 6a & b). MTMR4 knockdown prevented starvation-induced increases in dephosphorylated TFEB and the ratio of dephosphorylated TFEB/total TFEB compared with control cells. The protein kinase mTORC1 is the major enzyme that phosphorylates TFEB (Settembre et al., 2012). In both control and MTMR4-depleted cells, mTORC1 activity as evaluated by endogenous phosphorylation of the cellular mTORC1 substrates 4E-BP1 and

p85/p70 S6K was much lower in the starved condition compared with the fed condition (Fig. 6a). Detailed time-course analyses showed that the ratio of dephosphorylated TFEB/total TFEB was lower in MTMR4-depleted cells than in control cells with similar suppression of mTORC1 activity throughout the observation period of 8 h (Fig. 6c). Therefore, the failure of starvation-induced TFEB nuclear translocation (Fig. 5a & b) and the lower dephosphorylated TFEB ratio (Fig. 6b) in MTMR4-depleted cells are unlikely to be due to altered mTORC1 activity.

The Ca²⁺/calmodulin-dependent serine/threonine protein phosphatase, calcineurin, is implicated in dephosphorylation of TFEB (Medina et al., 2015). We treated the cells with the calcineurin inhibitor cyclosporine A (CsA) and studied starvation-induced dephosphorylation of TFEB. CsA did not affect the TFEB phosphorylation state under the starved condition in either control or MTMR4-depleted cells, suggesting that calcineurin was unlikely to be involved in the difference in the starvation-induced phosphorylation change of TFEB in control and MTMR4-depleted cells (Fig. 6d). In addition, starvation induced a decrease in MTMR4 but not MTMR3. The reduction of MTMR4 protein may have been due to increased autophagic degradation (Fig. 6a).

Because TFEB phosphorylation was reported to occur on LYs (Settembre et al., 2013), we studied in more detail the effect of MTMR4 depletion on the subcellular localization of TFEB with a time-lapse live-cell imaging technique. GFP-TFEB in non-treated fed cells was distributed largely in the cytoplasm in diffuse homogenous and fine granular patterns with enriched accumulation in the perinuclear region (green arrow in Fig. 7a). In contrast, in MTMR4-depleted cells, GFP-TFEB was distributed in the cytoplasm not only in a diffuse homogenous pattern but also in a coarse punctate pattern. Moreover, perinuclear enrichment of GFP-TFEB was not observed

in MTMR4-depleted cells, different from control cells. Addition of the mTOR inhibitor Torin1 to control cells resulted in rapid accumulation of GFP-TFEB in the nucleus with a reduction in the diffuse cytoplasmic pool, whereas the treatment induced only marginal and delayed GFP-TFEB nuclear accumulation in MTMR4-depleted cells (Fig. 7a and video S3). In both control and MTMR4-depleted cells under both fed and starved conditions, GFP-TFEB was not enriched in LAMP1⁺ LYs (Fig. 7b left). Instead, in MTMR4-depleted cells but not control cells, substantial accumulation of GFP-TFEB in Rab7⁺ LEs was observed (Fig. 7b right). Different from MTMR4, MTM1 knockdown failed to affect changes in the subcellular TFEB localization. MTMR4-KD induced accumulation of GFP-TFEB in PI(3)P-enriched structures under the fed condition, and this was further enhanced by starvation (Fig. S5). These data indicate that MTMR4 knockdown-induced change in TFEB phosphorylation is accompanied by changes in the subcellular localization of TFEB.

3 DISCUSSION

In this study, we demonstrated that MTMR4 is localized mainly in LEs and LC3B⁺ compartments (APs and ALYs) to regulate PI(3)P levels in these organelles and plays a critical role in the regulation of vesicular trafficking and maturation in the endocytic and autophagic pathways. MTMR4 also controls phosphorylation of TFEB, its nuclear translocation and consequently TFEB-dependent gene expression to regulate lysosomal and autophagic integrity. Thus, our study has revealed an essential role of MTMR4 in maintaining the functions of endocytic and autophagic pathways (Fig. 8).

MTMR4 knockdown resulted in increased accumulation of PI(3)P in endosomes, as indicated by the findings of FYVE signal-positive enlarged EEs and LEs compared with control cells (Fig. 2). Since MTMR4 is located predominantly in LEs (Fig. 1d & e and Fig. S1), the above data suggest that MTMR4 is a critical regulator controlling endosomal PI(3)P levels. Phosphoinositides regulate compartment-specific membrane trafficking through the mechanisms by which phosphoinositides recruit cytoplasmic effector proteins on specific membrane compartments (Falkenburger et al. 2010). Rapid production and elimination of phosphoinositides by specific phosphoinositide-metabolizing enzymes (phosphoinositide-kinases and –phosphatases) regulate the recruitment of phosphoinositide effector proteins (Billcliff et al., 2014; Liu et al., 2010; Marat et al., 2016). The EE-specific Rab protein, Rab5, recruits the class III phosphoinositide 3-kinase, Vps34, to facilitate the production of endosomal PI(3)P (Lindmo et al., 2006). PI(3)P is dephosphorylated to PI by MTMR4 and possibly other PI-3'-specific phosphatases and converted to PI (3,5)P₂ by PIKfyve in EEs and LEs (Dove et al., 2009; Hnia et al., 2012; Schink et al., 2013). PI(3)P, in concert with Rab5, recruits effectors including EEA1, which is required for docking and fusion of EEs and other vesicles. Thus, the proper turnover of

phosphoinositides is necessary for the initiation and termination of membrane trafficking events. We observed that MTMR4 depletion hampered the motility, fusion and fission of endosomes (Fig. S2). Therefore, it is likely that the appearance of enlarged PI(3)P-enriched EEs and LEs is due to the defective fusion and fission of organelle compartments along the endocytic pathway. Furthermore, the reductions in the numbers of LEs and LYs in MTMR4-depleted cells strongly suggest that MTMR4 is required for precise early-to-late endosome conversion and LE-LY fusion or the maturation of EEs and LEs toward LYs. Previous studies (Naughtin et al., 2010) showed in COS1 cells that MTMR4 overexpression delayed the exit of transferrin from EEs and its recycling to the plasma membrane, whereas MTMR4 knockdown led to unregulated translocation of Rab11-positive recycling endosomes, suggesting a role of MTMR4 in sorting of cargos from early endosomes. Our data and these previous findings collectively suggest that MTMR4 plays a role in early-to-sorting endosomal trafficking and the vesicular maturation of EEs to LEs and LYs along the endocytic pathway.

MTMR4 is also located in LC3B⁺ vesicles (Fig. 1e & f), suggesting its role in autophagy. A recent siRNA-based screen identified MTMR14 (jumpy) as a MTMR to regulate autophagic process (Vergne et al., 2009). MTMR14 associated with autophagic isolation membranes to exert a negative regulation for autophagosome formation at an early stage of autophagy. Another study (Taguchi-Atarashi et al., 2010) uncovered a negative regulatory role of MTMR3 in autophagosome formation. Further studies (Hao et al., 2016) showed that MTMR3 associated with mTOR and suppressed its activity in manners independent of MTMR3 enzymatic activity, suggesting the bimodal actions of MTMR3 in the autophagy regulation. Notably, MTMR3 was found to interact with MTMR4 in cells. In contrast to the effects of

knockdown of MTMR14 or MTMR3, MTMR4 knockdown rather induced reductions in the numbers of APs/ALYs and the autophagic flux with the lysosomal dysfunction through the mechanisms including TFEB inhibition (Fig. 2e, Fig. 3, and Fig. 5a). Thus, it appears that the MTMR members exert isoform-specific distinct regulatory roles in autophagy by the mechanisms including the isoform-specific subcellular localization and interaction with other MTMR members.

A549 cells are derived from alveolar type II epithelium, which synthesizes pulmonary surfactant lipid-protein complex, stores it in LBs, and secretes it at the plasma membrane (Kondo et al., 2015; Robin et al., 2010; Wang, et al., 2002). LBs express lysosomal markers and are now recognized as secretory lysosomes or lysosome-related organelles. MTMR4 knockdown induced an increase in LBs in A549 cells (Fig. S3), suggesting that MTMR4 may also regulate the formation, trafficking and/or fusion of LBs. Further studies are required to understand how MTMR4 exactly regulates LBs.

TFEB regulates autophagy and lysosomal biogenesis through transcriptionally stimulating the expression of genes involved in these two processes, and thereby contributes to metabolic homeostasis. Although the transcriptional activity of TFEB is regulated by its serine phosphorylation (Martina et al., 2012), the overall mechanisms by which TFEB activity in cells is regulated are not well understood. In this study, MTMR4 knockdown induced an increase in the amount of total TFEB, particularly the phosphorylated form of TFEB, resulting in a reduced ratio of dephosphorylated TFEB/total TFEB (Fig. 6b). The phosphorylated form of TFEB by itself is inactive and further reduces TFEB activity by forming heterodimers with dephosphorylated, active TFEB to decrease nuclear translocation of dephosphorylated TFEB (Sha et al., 2017). Thus, phosphorylated TFEB exerts a dominant-negative action. The

phosphorylated form of TFEB was also shown to undergo degradation by the ubiquitin-proteasome system. How MTMR4 controls the amount of phosphorylated TFEB and its turnover remains to be clarified. Another observation of interest in this study was MTMR4 knockdown–induced change in the subcellular distribution of TFEB, i.e., the accumulation of TFEB in Rab7⁺, PI(3)P–enriched LEs in MTMR4–depleted cells (Fig. 7 and Fig. S5). The molecular mechanisms for the altered subcellular TFEB distribution upon MTMR4 depletion also remain to be revealed. Phosphorylation of TFEB is known to occur normally in LYs (Roczniak-Ferguson et al., 2012; Settembre et al., 2013). The localization change of TFEB may somehow affect efficiency of mTOR–mediated phosphorylation and/or calcineurin–mediated dephosphorylation and, thereby, TFEB activity.

Taken together, our study indicates that MTMR4 deficiency disturbs endosomal traffic, the maturation of EEs toward LEs and LYs, and the progress of autophagy through the impairment of appropriate elimination of PI(3)P in the organelle membrane and TFEB activation required for autophagy and lysosomal biogenesis. Thus, MTMR4 is essential for the integrity of the endocytic and autophagic pathways.

4 EXPERIMENTAL PROCEDURES

4.1 Cell culture, transfection and reagents

A549 (human adenocarcinoma epithelial cell line), HeLa, HEK293T and mouse embryonic fibroblast (MEF) cells were cultured in Dulbecco's Modified Eagle Medium (DMEM, high glucose, Wako Pure Chemical) supplemented with 10% fetal bovine serum (FBS, Sigma), 2 mM L-glutamine, 100 units/ml penicillin (Wako Pure Chemical) and 100 µg/ml streptomycin (Wako Pure Chemical) at 37°C under 5% CO₂. Human umbilical vein endothelial cells (HUVEC, #C2517A, Lonza), lung microvascular endothelial cells (HMVEC-L, #CC-2527, Lonza) and aortic vascular smooth muscle cells (HAoVSM, #CC-2571, Lonza) were maintained according to the manufacturer's instructions. Mouse lung vascular endothelial cells (MLVEC), aortic vascular smooth muscle cells (MAoVSM) and skin fibroblast cells (MSF) were isolated from adult C57BL6/J mice and cultured as previously described (Yoshioka et al., 2012; Aki et al., 2015). For knockdown of endogenous MTMR4 and other isoforms with small interference RNA (siRNA), cells were transiently transfected with Lipofectamine RNAiMAX (#13778, Invitrogen-Thermo Fisher Scientific) in Opti-MEM (#31985070, Gibco-Thermo Fisher Scientific) according to the manufacturer's instructions for 48-72 h before the experiments. The target sequences were: 5'- AACCACAUCUGGUU CUUUC -3' for human MTMR4; 5'- UUUCUAUAAGCUGUAAUGG -3' for human MTMR3; 5'- UUCGAGAUGCAAUUAUG -3' for human MTM1; and 5'- AAACUCAACACUGG CUAUUA-3' for human Vps34. As a control, MISSION siRNA Universal Negative Controls were used (#SIC001, Sigma-Aldrich). Efficiency of RNA interference was confirmed by Western blotting using specific antibodies. For treatment with Torin1, chloroquine and MG-132, the final concentrations were

250 nM, 100 μ M and 10 μ M, respectively, unless otherwise stated. For nutrient starvation, cells were incubated in HBSS without serum for 4 h unless otherwise stated.

The expression vectors for the siRNA-resistant GFP-R4^r and the siRNA-resistant, catalytically inactive GFP-C407S-R4^r were generated using a standard PCR-based method. In brief, GFP-R4^r was generated by introducing silent mutations in the human MTMR4 sequence using the following mutations: the codons GGA-AAG-AAC-CAG for the amino acids Gly⁹⁷⁷-Lys⁹⁷⁸-Asn⁹⁷⁹-Gln⁹⁸⁰ were replaced by the nucleotides GGG-AAA-AAT-CAA, which encodes the same amino acids. GFP-C407S-R4^r was generated by a point mutation at the conserved catalytic site of the phosphatase domain (Laporte, 2003). All mutants were constructed by PrimeSTAR site-directed Mutagenesis Basal Kit (#R046A, Takara) and confirmed by DNA sequencing (Takara). The expression vectors for GFP-2xFYVE and mRFP-2xFYVE were described previously (Yoshioka et al., 2012). The expression vectors for GFP-2xML1N and mCherry-2xML1N were provided by Dr. Haoxing Xu (University of Michigan) (Li et al., 2013). GFP-TFEB expression vector (# 38119) was provided by Dr. Shawn Ferguson through Addgene (Roczniak-Ferguson et al., 2012). To establish A549 cells stably expressing the mRFP-2xFYVE domain, cells were transfected with electroporation using the Amaxa Nucleofector-based system (Program X- 001, Lonza) and selected with 500 μ g/ml G418 sulfate (Geneticin, #11811-023, Roche-Life Technologies). Chloroquine (C-6628) was obtained from Sigma. N-carbobenzoxy-Leu-Leu-norleucinal (MG-132, #474790) and Torin1 were purchased from Calbiochem-Merck. All other reagents were purchased from Sigma unless otherwise indicated.

4.2 Immunostaining and confocal microscopy

Cells were grown on type-I collagen (Nitta gelatin)-coated coverslips (Matsunami Glass) or glass-bottom dishes (MatTek Corporation) and allowed to adhere to dishes in growth medium overnight. Cells were rinsed with pre-warmed Ca^{2+} - and Mg^{2+} -free Dulbecco's phosphate buffered saline (PBS) once and fixed with 4% paraformaldehyde (PFA) in 0.1M phosphate buffer (pH7.4) at room temperature for 10 min, washed with PBS and then permeabilized and blocked in 5% normal goat serum (NGS)/0.3% Triton X-100 in PBS. The cells were stained with the indicated primary antibodies at 4°C overnight. The antibodies used were against MTMR4 (catalog #AP6804a, Abgent), TFEB (#4240S, CST), Rab7 (#9367, CST), LAMP1 (#328602, BioLegend), CD63 (also known as LAMP3, #CBL55, Millipore), LC3B (#3868S, CST), P62 (#8025S, CST), EEA1 (#610456, BD), ABCA3 (#LS-346373, LSBio), Rab11 (#5589, CST), PPP3CB (#GTX104088, Gentex). After washes with 0.1% TritonX-100 in PBS three times, cells were incubated with Alexa Fluor-conjugated secondary antibodies (Molecular Probes-Thermo Fisher Scientific) diluted at 1:1000 in 0.1% TritonX-100 for 1 h at room temperature.

Where appropriate, cells were counterstained with DAPI (# D1306, Molecular Probe, Thermo Fisher) for 15 min. Cells were mounted on Fluoromount (K024, Diagnostic BioSystems) and imaged under a custom confocal microscope unit as described in detail previously (Yoshioka et al., 2012; Biswas et al., 2013; Aki et al., 2015). For quantification of positive pixels, the positive area, and colocalization index (Pearson's correlation coefficient) in stained images in each frame was calculated using Image-J/Fiji software.

4.3 Live-cell imaging

Live-cell imaging was performed as described previously (Yoshioka et al., 2012). In brief, mRFP-2xFYVE- and mCherry-2xML1N-expressing cells were plated on collagen-coated glass-bottom dishes (MatTek, # P35G-1.5-20-C). Cells on a heated stage (37°C; Tokai-Hit) were observed under a custom confocal microscope based on an inverted IX70 microscope (Olympus) equipped with an UPLSAPO 60X/NA1.35-oil objective, a confocal disk-scan unit (CSU10, Yokogawa), an EM-CCD digital camera (iXon, Andor) and a light engine (Lumencor, Inc.) for 3D time-lapse confocal imaging. The acquisition and process were controlled by iQ software (Andor). Images were taken at every 5-s interval, and movies were prepared at a frequency of 20 frames/s. To examine the cellular acidic compartment, cells were incubated with LysoTracker-red (50 nM, # L7528, Molecular Probes, Thermo Fisher Scientific) for 30 min before observations with a confocal microscope.

4.4 Imaging of mRFP-GFP-LC3B autophagy sensor-expressing cells

Cells transfected with the mRFP-GFP-LC3B tandem probe expression vector (# P36239, Molecular Probes, Thermo Fisher Scientific) were grown overnight on collagen-coated glass-bottom dishes according to the manufacturer's instructions. Autophagy was induced by starvation by incubating cells in HBSS with or without 100 μ M chloroquine for 4 h, or by incubating cells for 4h in growth medium with 250 nM of the mTOR inhibitor Torin1. Cells were fixed with 4% PFA, washed with PBS, counterstained with DAPI, and mounted using Fluoromount. Images were acquired randomly by confocal microscopy as described above. Cells were outlined manually, and each channel was independently thresholded using the same setting across all images from each channel. mRFP and GFP puncta, colocalized puncta and total mRFP-GFP-LC3B fluorescence were quantified using ImageJ/Fiji software.

4.5 FITC-dextran uptake and degradation assay

At 48 h after siRNA transfection, cells were pulsed with 0.2 mg/ml concentration of FITC-dextran (70-kDa M.W., Sigma FD70S) in growth medium at 37 °C for 1 h, washed 3 times with growth medium, and were returned to the CO₂ incubator. At the indicated time point, cells were fixed with 4% PFA for 15 min and stained with DAPI. Cells were imaged under a custom confocal microscope unit as described above.

4.6 Western blotting

At 48 h after siRNA transfection, cells were starved in HBSS in the presence or absence of chloroquine for 4 h, washed in PBS and then lysed in RIPA buffer (1% Triton X-100, 0.5 % sodium deoxycholate, 0.1 % SDS, 25 mM Tris-HCl, pH 7.4, 150 mM NaCl, 10 mM NaF, 10 mM β-glycerophosphate, 1m M Na₃VO₃, 5 mM EDTA, and protease inhibitor cocktail (Complete Mini, Roche)) or ice-cold 2x Laemmli sample buffer. The samples were centrifuged at 15,000 *xg* for 5 min at 4°C after boiling at 100°C for 5 min. The resultant supernatants were recovered and resolved by 8-12.5 % SDS-PAGE, followed by electrotransfer onto PVDF membrane (Millipore-Merck) using Trans-Blot Turbo blotting systems (Bio-Rad). The membranes were blocked in blocking solution (TOYOBO) for 1 h and probed with respective antibodies. The antibodies used were against MTMR4 (1:400, #AP6804a, Abgent), MTMR3 (1:1000, #12443S, Cell Signaling Technology(CST)), TFEB (1:1000, #4240S, CST), Rab7 (1:1000, #9367, CST), LC3B (1:1000, #3868S, CST), p62 (1:1000, #8025S, CST), 4EBP1 (1:1000, #2855P, CST), 4EBP1-P (1:1000, Thr37/46, #2855, CST), S6K (1:1000, #9234S, CST), phospho-S6K (1:1000, S371, #9208P, CST), PI3K-C2α (1:1000, #12402S, CST), GAPDH (1:2000, #016-25523, Wako), and β-actin (1:1000, #013-24553, Wako). After incubation with the appropriate

alkaline phosphatase–conjugated secondary antibodies (1:1000, anti-rabbit IgG: #7054, anti-mouse IgG: #7056, CST), protein bands were visualized by the color reaction using the nitro blue tetrazolium (NBT, WAKO)/5-bromo-4-chloro-3'-indolylphosphate *p*-toluidine (BCIP, WAKO) system. Band intensity of western blotting was determined using Image Studio lite software (LI-COR). The quantified values were normalized for the value of GAPDH or β -actin as a loading control and expressed as multiples over the normalized values of controls.

4.7 Quantitative real-time PCR with reverse transcription (qRT-PCR)

Total RNA was isolated from cells using TRIzol reagent (Invitrogen). One microgram of total RNA was treated with DNase (Qiagen) to eliminate genomic DNA and reverse-transcribed into first strand cDNA using a QuantiTect RT kit (#205313, Qiagen). Quantification of gene expression was performed using an ABI-7300 qPCR thermal cycler (Applied Biosystems, Inc.) in duplicate. Primer sequences are listed in Supplementary Table 1. We have validated that these primer pairs are highly specific for each target without cross-amplification. Comparison of relative gene expression was performed by the $\Delta\Delta C_t$ method with normalization of raw data to a housekeeping gene, as previously described (Yoshioka et al., 2012).

4.8 Flow cytometry

A549 cells were transfected with control siRNA or sMTMR4 and cultured for 48 h. Then, cells were incubated with LysoTracker-red (50 nM) for 30 min. After treatment, cells were harvested by trypsinization, and washed twice with ice–cold PBS. Then, cells were suspended in Cytofic/Cytoperm (BD) and incubated for 30 min on ice.

Cells were washed twice with ice-cold PBS and resuspended in 2% FBS/PBS, and analyzed with a flow cytometer (BD FACS Aria-II cell sorter).

4.9 Transmission electron microscopy

Cells were fixed by immersion in 2% PFA plus 2% glutaraldehyde in 30 mM HEPES buffer (pH 7.4) for 30 min at 4°C, and post-fixed in 1% osmium tetroxide for 1 h at 4°C. They were then dehydrated through a graded ethanol series, and embedded in epoxy resin. Ultrathin sections were stained with 1% uranyl acetate for 30 min followed by Reynolds lead citrate for 5 min, and then subjected to observation with a Hitachi H-7650 electron microscope.

4.10 Statistical analysis

Statistical analysis was performed with GraphPad Prism 7 software (GraphPad Software). Data are presented as mean \pm standard error of mean (SEM). Statistical significance was evaluated with two-tailed unpaired Student's *t*-test or one-way ANOVA followed by Bonferroni post-hoc test unless stated otherwise. $P < 0.05$ was considered to indicate statistical significance.

ACKNOWLEDGMENTS

We thank Ms. Chiemi Hirose for secretarial assistance. This study was supported by grants from the Ministry of Education, Science, Sports and Culture of Japan, and the Japan Society for the Promotion of Science.

REFERENCES

- Aki, S., Yoshioka, K., Okamoto, Y., Takuwa, N., & Takuwa Y. (2015). Phosphatidylinositol 3-kinase class II α -isoform PI3K-C2 α is required for transforming growth factor β -induced Smad signaling in endothelial cells. *J. Biol. Chem.*, 290(10), 6086-6105. <https://doi.org/10.1074/jbc.M114.601484>
- Al-Qusairi, L., Prokic, J., Amoasii, L., Kretz, C., Messaddeq, N., Mandel, J-L., & Laporte, J. (2013). Lack of myotubularin (MTM1) leads to muscle hypertrophy through unbalanced regulation of the autophagy and ubiquitin-proteasome pathways. *FASEB J.*, 27(8), 3384-3394. <https://doi.org/10.1096/fj.12-220947>
- Armi, C.D., Devereaux, K.A., & Di Paolo, G. (2013). The role of lipids in the control of autophagy. *Curr. Biol.*, 23(1), R33-45. <https://doi.org/10.1016/j.cub.2012.10.041>
- Azzedine, H., Bolino, A., Taieb, T., Birouk, N., Di Duca, M., Bouhouche, A., Benamou, S., Mrabet, A., Hammadouche, T., Chkili, T., Gouider, R., Ravazzolo, R., Brice, A., Laporte, J., & LeGuern, E. (2003). Mutations in MTMR13, a new pseudophosphatase homologue of MTMR2 and Sbf1, in two families with an autosomal recessive demyelinating form of Charcot-Marie-Tooth disease associated with early-onset glaucoma. *Am. J. Hum. Genet.*, 72(5), 1141-1153. <https://doi.org/10.1086/375034>
- Balla, T. (2013). Phosphoinositides; tiny lipids with giant impact on cell regulation. *Physiol. Rev.*, 93(3), 1019-1137. <https://doi.org/10.1152/physrev.00028.2012>
- Billcliff, P.G., & Lowe, M. (2014). Inositol lipid phosphatases in membrane trafficking and human disease. *Biochem. J.*, 461 (2), 159-175. <https://doi.org/10.1042/BJ20140361>
- Biswas, K., Yoshioka, K., Asanuma, K., Okamoto, Y., Takuwa, N., Sasaki, T., & Takuwa, Y. (2013). Essential role of class II phosphatidylinositol-3-kinase-C2 α in sphingosine 1-phosphate receptor-1-mediated signaling and migration in endothelial cells. *J. Biol. Chem.*, 288(4), 2325-2339. <https://doi.org/10.1074/jbc.M112.409656>
- Carlsson, S.R., & Simonsen, A. (2015). Membrane dynamics in autophagosome biogenesis. *J Cell Sci.*, 128(2), 193-205. <https://doi.org/10.1242/jcs.141036>
- Vergne, I., Roberts, E., Elmaoued, R.A., Tosch, V., Delgado, M.A., Proikas-Cezanne, T., Laporte, J., & Deretic, V. (2009). Control of autophagy initiation by phosphoinositide 3-phosphatase jumpy. *EMBO J.* 28(7), 2244–2258. <https://doi.org/10.1016/j.febslet.2010.02.054>
- Fratti, RA., Backer, JM., Gruenberg, J., Corvera, S., & Deretic, V. (2001). Role of phosphatidylinositol 3-kinase and Rab5 effectors in phagosomal biogenesis and mycobacterial phagosome maturation arrest. *J. Cell Biol.*, 154(3), 631-644. <https://doi.org/10.1083/jcb.200106049>

Hao, F., Itoh, T., Morita, E., Shirahama-Noda, K., Yoshimori, T., & Noda, T. (2016). The PtdIns3-phosphatase MTMR3 interacts with mTORC1 and suppresses its activity. *FEBS Letters*, 590(1), 161-173. <https://doi.org/10.1002/1873-3468.12048>

Hnia, K., Vaccari, I., Bolino, A., & Laporte, J. (2012). Myotubularin phosphoinositide phosphatase: cellular functions and disease pathophysiology. *Trends Mol. Med.*, 18(6), 317-327. <https://doi.org/10.1016/j.molmed.2012.04.004>

Huotari, J. and Helenius, A. (2011). Endosome maturation. *EMBO J.*, 30(17), 3481-3500. <https://doi.org/10.1038/emboj.2011.286>

Ketal, K., Krauss, M., Nicot, A.S., Puchkov, D., Wieffer, M., Muller, R., Subramanian, D., Schultz, C., Laporte, J., & Haucke, V. (2016). A phosphoinositide conversion mechanism for exit from endosomes. *Nature*, 529(7586), 408-412.

Kimura, S., Noda, T., and Yoshimori, T. (2007). Dissection of the autophagosome maturation process by a novel reporter protein, tandem fluorescent-tagged LC3. *Autophagy*, 3(5), 452-460. <https://doi.org/10.4161/auto.4451>

Kioschis, P., Rogner, UC., Pick, E., Klauck, SM., Heiss, N., Siebenhaar, R., Korn, B., Coy, JF., Laporte, J., Liechti-Gallati, S., & Poustka, A. (1996). A 900-kb cosmid contig and 10 new transcripts within the candidate region for myotubular myopathy (MTM1). *Genomics*, 33(3), 365-373. <https://doi.org/10.1006/geno.1996.0212>

Komatsu, M., & Ishimura, Y. (2010). Selective autophagy regulates various cellular functions. *Genes Cells.*, 15(9), 923-933. <https://doi.org/10.1111/j.1365-2443.2010.01433.x>

Kondo, H., Miyoshi, K., Sakiyama, S., Tangoku, A., & Noma, T. (2015). Differential Regulation of gene expression of alveolar epithelial cell markers in human lung adenocarcinoma-derived A549 clones. *Stem Cell Int.*, 2015, 165867. <https://doi.org/10.1155/2015/165867>

Li, C., Kita, A., Hashimoto, Y., Ihara, M., Kato, A., Ogura, N., Doi, A., Oku, M., Itoh, T., Sakai, Y., & Sugiura, R., (2013). Functional link between Rab GTPase-mediated membrane trafficking and PI4,5P2 signaling. *Genes. Cells.*, 19(3), 177-197. <https://doi.org/10.1111/gtc.12123>

Li, X., Wang, X., Zhang, X., Zhao, M., Tsang, WL., Zhang, Y., Yau, R.G., Weisman, L.S., & Xu, H. (2013). Genetically encoded fluorescent probe to visualize intracellular phosphatidylinositol 3,5-bisphosphate localization and dynamics. *Proc. Natl. Acad. Sci. USA*, 110(52), 21165-21170. <https://doi.org/10.1073/pnas.1311864110>

Liu, J., Lv, Y., Liu, Q-h., Qu, C-K., & Shen, J. (2014). Deficiency of MTMR14 promotes autophagy and proliferation of mouse embryonic fibroblasts. *Mol. Cell. Biochem.*, 392(1-2), 31-37. <https://doi.org/10.1007/s11010-014-2015-5>

Liu, Y., & Bankaitis, V.A. (2010). Phosphoinositide phosphatases in cell biology and disease. *Prog. Lipid Res.* 49(3), 201-217.

<https://doi.org/10.1016/j.plipres.2009.12.001>

Lorenzo, O., Urbe S., & Clague, M. J. (2005). Systematic analysis of myotubularins: heteromeric interactions, subcellular localization and endosome- related functions. *J. Cell Sci.*, 119, 2953-2959. <http://doi: 10.1242/jcs.03040>

Marat, A.L., & Haucke, V. (2016). Phosphatidylinositol 3-phosphates—at the interface between cell signalling and membrane traffic. *EMBO J.*, 35(6), 561-579.

<https://doi.org/10.15252/emj.201593564>

Martina, J. A., Chen, Y., Gucek, M., Puertollano, R. (2012). MTORC1 functions as a transcriptional regulator of autophagy by preventing nuclear transport of TFEB.

Autophagy, 8(6), 903-914. <https://doi.org/10.4161/auto.19653>

Medina, D.L., Di Paola, S., Peluso, I., Armani, A., De Stefani, D., Venditti, R., Montefusco, S., Scotto-Rosato, A., Prezioso, C., Forrester, A., Settembre, C., Wang, W., Gao, Q., Xu, H., Sandri, M., Rizzuto, R., De Matteis, M.A., & Ballabio, A.

(2015). Lysosomal calcium signaling regulates autophagy through calcineurin and TFEB. *Nat. Cell Biol.*, 17(3), 288-299. <https://doi.org/10.1038/ncb3114>

Mizushima, N., Yoshimori, T., & Ohsumi, Y. (2011). The role of Atg proteins in autophagosome formation. *Annu. Rev. Cell Dev. Biol.*, 27, 107-132.

<https://doi.org/10.1146/annurev-cellbio-092910-154005>

Mu, F.T., Callaghan, J.M., Steele-Mortimer O., Stenmark, H., Parton, R.G., Campbell, P.L., McCluskey, L., Yeo, J.P., Tock, E.P., Toh, B.H., (1995). EEA1, an early endosome-associated protein. EEA1 is a conserved alpha-helical peripheral membrane protein flanked by cysteine 'fingers' and contains a calmodulin binding IQ motif. *J. Biol. Chem.*, 270(22), 13503–13511.

<https://doi.org/10.1074/jbc.270.22.13503>

Naughtin, M.J., Sheffield, D.A, Rahman, P., Hughes, W.E., Gurung, R., Stow, J.L., Naudurkar, H.H., Dyson, J.M., & Mitchell, C.A. (2010). The myotubularin phosphatase MTMR4 regulates sorting from early endosomes. *J. Cell. Sci.*, 123(Pt 18), 3071-3083.

<https://doi.org/10.1242/jcs.060103>

Nascimbeni, A.C., Codogno, P., & Morel, E. (2016). Phosphatidylinositol-3-phosphate in the regulation of autophagy membrane dynamics. *FEBS J.*, 284(9), 1267-1278.

<https://doi.org/10.1111/febs.13987>

Noda, T., Matsunaga, K., Taguchi-Atarashi, N., Yoshimori, T. (2010)., Regulation of membrane biogenesis in autophagy via PI3P dynamics. *Semin Cell. Dev. Biol.*, 21(7), 671-676.

<https://doi.org/10.1016/j.semcdb.2010.04.002>

Plant, P.J., Correa, J., Goldenberg, N., Bain J., & Batt, J. (2009). The inositol phosphatase MTMR4 is a novel target of the ubiquitin ligase Nedd4. *Biochem. J.* 419(1), 57-63. <https://doi.org/10.1042/BJ20081866>

Robin J. Swain, Sarah J. Kemp, Peter Goldstraw, Teresa D. Tetley, Molly M. Stevens. (2010). Assessment of cell line models of primary human cells by raman spectral phenotyping. *Biophys. J.* 98(8), 1703-1711. <https://doi.org/10.1016/j.bpj.2009.12.4289>

Roczniak-Ferguson, A., Petit, C.S., Froehlich, F., Qian, S., Ky, J., Angarola, B., Walther, T.C., & Ferguson, S.M. (2012). The transcription factor TFEB links mTORC1 signaling to transcriptional control of lysosome homeostasis. *Sci. Signal.*, 5(228), ra42. <https://doi.org/10.1126/scisignal.2002790>

Sardiello, M., Palmieri, M., Di Ronza, A., Medina, D.L., Valenza, M., Gennarino, V.A., Di Malta, C., Donaudy, F., Embrione, V., Polishchuk, R.S., Banfi, S., Parenti, G., Cattaneo, E., & Ballabio, A. (2009). A gene network regulating lysosomal biogenesis and function. *Science*, 325(5939), 473-477. <https://doi.org/10.1126/science.1174447>

Schink, K.O., Raiborg, C., & Stenmark, H. (2013). Phosphatidylinositol 3-phosphate, a lipid that regulates membrane dynamics, protein sorting and cell signaling. *Bioessays*, 35(10), 900-912. <https://doi.org/10.1002/bies.201300064>

Settembre, C., Di Malta, C., Polito, V.A., Garcia Arencibia, M., Vetrini, F., Erdin, S., Erdin, S.U., Huynh, T., Medina, D., Colella, P., Sardiello, M., Rubinsztein, D.C., & Ballabio, A. (2011). TFEB links autophagy to lysosomal biogenesis. *Science*, 332(6036), 1429-1433. <https://doi.org/10.1126/science.1204592>

Settembre, C., Zoncu, R., Medina, D.L., Vetrini, F., Erdin, S., Erdin, S., Huynh, T., Ferron, M., Karsenty, G., Vellard, M.C., Facchinetti, V., Sabatini, D.M., & Ballabio, A. (2012). A lysosome-to-nucleus signalling mechanism senses and regulates the lysosome via mTOR and TFEB. *EMBO J.*, 31(5), 1095-1108. <https://doi.org/10.1038/emboj.2012.32>

Settembre, C., Fraldi, A., Medina, D.L., & Ballabio, A. (2013). Signals from the lysosome: a control centre for cellular clearance and energy. *Nat. Rev. Mol. Cell Biol.*, 14(5), 283-296. <https://doi.org/10.1038/nrm3565>

Sha, Y., Rao, L., Settembre, C., Ballabio, A., & Eissa, N.T. (2017) STUB1 regulates TFEB-induced autophagy-lysosome pathway. *EMBO J.*, 36(17), 2544-2552. <https://doi.org/10.15252/emboj.201796699>

Shen, H., Mizushima, N. (2013). At the end of the autophagic road: an emerging understanding of lysosomal functions in autophagy. *Cell*, 39(2), 61-71.

St-Denis, N., Gupta, G.D., Lin, Z.Y., Gonzalez-Badillo, B., Pelletier, L., & Gingras, A.C. (2016). Myotubularin-related protein 3 and 4 interact with polo-like kinase 1 and centrosomal protein of 55 kDa to ensure proper abscission. *Mol. Cell Proteomics.*, *14*(4), 946-960. <https://doi.org/10.1016/j.celrep.2016.10.078>

Taguchi-Atarashi, N., Hamasaki, M., Matsunaga, K., Omori, H., Ktistakis, N.T., Yoshimori, T., & Noda, T. (2010) Modulation of local PtdIns3P levels by the PI phosphatase MTMR3 regulates constitutive autophagy. *Traffic*, *11*, 468-478. <https://doi.org/10.1111/j.1600-0854.2010.01034>

Teo, W.X., Kerr, M.C., & Tesadale, R.D. (2016). MTMR4 is required for the stability of the Salmonella-containing vacuole. *Front. Cell. Infect. Microbiol.*, *6*, 91. <https://doi.org/10.3389/fcimb.2016.00091>

Vergne, I., & Deretic, V., (2010). The role of PI3P phosphatases in the regulation of autophagy. *FEBS Letter.*, *584*, 1313-1318. <https://doi.org/10.1016/j.febslet.2010.02.054>

Wallroth, A., & Haucke, V., (2017). Phosphoinositide conversion in endocytosis and the endolysosomal system. *J. Biol. Chem.*, *293*(5), 1526-1535. <https://doi.org/10.1074/jbc.R117.000629>

Wang, W.J., Russo, S.J., Muligeta, S., & Beers, M.F. (2002). Biosynthesis of surfactant protein C (SP-C). Sorting of SP-C proprotein involves homomeric association via a signal anchor domain. *J. Biol. Chem.*, *277*(22), 19929-19937. <https://doi.org/10.1074/jbc.M201537200>

Yoshioka, K., Yoshida, K., Cui, H., Wakayama, T., Takuwa, N., Okamoto, Y., Du, W., Qi, X., Asanuma, K., Sugihara, K., Aki, S., Miyazawa, H., Biswas, K., Nagakura, C., Ueno, M., Iseki, S., Schwartz, R.J., Okamoto, H., Sasaki, T., Matsui, O., Asano, M., Adams, R.H., Takakura, N., & Takuwa, Y. (2012). Endothelial PI3K-C2 α , a class II PI3K, has an essential role in angiogenesis and vascular barrier function. *Nat. Med.* *18*(10), 1560-1569. <https://doi.org/10.1038/nm.2928>

Zou, J., Zhang, C., Marjanovic, J., Kisseleva, M.V., Majerus, P.W., & Wilson, M.P. (2012). Myotubularin-related protein (MTMR) 9 determines the enzymatic activity, substrate specificity, and role in autophagy of MTMR8. *Proc. Natl. Acad. Sci. USA.*, *109*(24), 9539-9544. <https://doi.org/10.1073/pnas.1207021109>

FIGURE LEGENDS

FIGURE 1. MTMR4 localizes mainly to late endosomes and autophagosomes in

A549 cells. (a) MTMR4 protein expression in various human and mouse cells.

MTMR4 expression was determined by Western blot analysis with GAPDH as a

loading control. HUVEC: human umbilical endothelial cells, HMVEC: human

microvascular endothelial cells, HASMC, human aortic smooth muscle cells, MEF,

mouse embryonic fibroblasts, MLEC, mouse lung vascular endothelial cells,

MASMC, mouse aortic smooth muscle cells, MSF, mouse skin fibroblasts. **(b)**

Specific siRNA-mediated knockdown of MTMR4 protein expression in A549 cells.

Cells were transfected with MTMR4-specific siRNA or control siRNA and 48 h later

underwent Western blot analysis using anti-MTMR4, -MTMR3, or -PI3K-C2 α

antibodies. β -actin was analyzed as a loading control. **(c)** Immunostaining of

MTMR4-depleted and control A549 cells. Cells were immunostained with anti-

MTMR4 antibody and observed with a confocal fluorescence microscope.

Representative images are shown. Scale bar: 10 μ m. **(d)** Co-localization of GFP-

MTMR4 and a lysosomal marker, PI(3,5)P₂ or PI(3)P. A549 cells were transfected

with the GFP-MTMR4 expression vector and loaded with LysoTracker-red (upper

panel), or co-transfected with the GFP-MTMR4 expression vector and either the

mCherry-2xML1N domain (PI(3,5)P₂-specific probe) (middle panel) or the mRFP-

2xFYVE domain (PI(3)P-specific probe) (lower panel) -expression vectors. Live-cell

imaging was performed as described in Experimental Procedures. Arrowheads

indicate colocalization. Scale bar: 20 μ m. **(e)** Co-localization of GFP-MTMR4 and

organelle markers. A549 cells were transfected with the GFP-MTMR4 expression

vector, followed by immunostaining using specific antibodies against EEA1 (EE),

Rab7 and CD63 (LE), Rab11(RE), LC3B (AP), LAMP1 (LY) and ABCA3 (LB).

Arrowheads indicate colocalization. Scale bar: 10 μ m. In (c) to (e), nuclei were stained with DAPI (blue). (f) Quantification of relative colocalization (Pearson's correlation coefficient) of GFP-MTMR4 with organelle markers.

FIGURE 2. MTMR4 knockdown enlarges PI(3)P-enriched EEs and LEs, and reduces LEs and LYs.

(a) Fluorescent images of mRFP-2xFYVE-expressing MTMR4-depleted and control A549 cells. (b) Fluorescent images of mCherry-2xML1N-expressing MTMR4-depleted and control A549 cells. In (a) and (b), cells that expressed mRFP-2xFYVE probe for PI(3)P or mCherry-2xML1N probe for PI(3,5)P₂ were live-imaged (see also Videos S1 and S2). Right panels in (a) and (b) show a histogram of the sizes of PI(3)P- and PI(3,5)P₂-enriched vesicles in control and MTMR4-depleted cells. (c-f) Immunostaining of A549 cells stably expressing mRFP-2xFYVE with antibodies against organelle-specific markers. (c) Anti-EEA1(EEs), (d) anti-Rab7 (LEs), (e) anti-LC3B (APs), and (f) anti-LAMP1 (LYs). Cells were observed with a confocal fluorescence microscope. Nuclei were counterstained with DAPI. Arrowheads indicate co-localized vesicles that give a yellow color. Right panels in (c) to (f) show quantified data of the numbers of organelle marker⁺ vesicles, colocalization index (Pearson's correlation coefficient), and relative vesicle size histogram (relative frequency %).

FIGURE 3. MTMR4 knockdown reduces APs and ALYs.

(a-b) Imaging of APs and ALYs with mRFP-GFP-LC3B autophagy sensor in control (upper panel) and MTMR4-depleted (lower panel) cells in both fed (a) and starved (b) conditions. A549 cells transfected with the mRFP-GFP-LC3B expression vector

were cultured in growth medium or Hanks' balanced salt solution (HBSS) for 4 h. The boxed regions in the merged images are magnified and shown in the right panels. Nuclei are stained with DAPI (blue) staining. Quantified data of mRFP⁺ GFP⁺ yellow dots (non-acidified APs) and mRFP⁺ GFP⁻ red dots (acidified, degradative ALYs) per cell, and relative vesicle size histogram (relative frequency %) are shown. (c) Transmission electron microscopy (TEM) images of control and MTMR4-depleted A549 cells in normal growth medium (fed) or HBSS (starved). The boxed regions in the merged images are magnified and shown in the right panels. Mito, mitochondria.

FIGURE 4. MTMR4 knockdown induces enrichment of PI(3)P in LC3B⁺ compartment and LEs upon starvation.

(a-b) Immunostaining of A549 cells stably expressing mRFP-2xFYVE with anti-LC3B (AP and ALY marker) antibody (a) and anti-Rab7 (LE marker) antibody (b). A549 cells stably expressing mRFP-2xFYVE that were transfected with control- or MTMR4-siRNAs were placed in growth medium (fed) or HBSS (starved) for 4 h. Nuclei were counterstained with DAPI. Immunostained cells were observed with a confocal microscope. Arrowheads indicate PI(3)P-enriched, LC3B⁺ or Rab7⁺ yellow vesicles. The right panels in (a) and (b) show the quantified data of the numbers of LC3B⁺ and Rab7⁺ dots and the colocalization index (Pearson's correlation coefficient).

FIGURE 5. MTMR4 knockdown inhibits starvation-induced nuclear translocation of TFEB.

(a) Starvation-induced nuclear translocation of GFP-TFEB in control and MTMR4- and MTM1-depleted cells. GFP-TFEB-expressing A549 cells that were transfected with the GFP-TFEB expression vector were placed in growth medium (fed) or HBSS

(starved) for 4 h. Nuclei were counterstained with DAPI. Immunostained cells were observed with a confocal microscope. Scale bar = 10 μm . (b) Quantified data of nuclear translocation of GFP-TFEB. (c) Starvation-induced nuclear translocation of endogenous TFEB in control and MTMR4- and MTM1-depleted cells. Cells were treated as in (a) and immunostained for TFEB. Scale bar = 10 μm . (d) Quantified data of nuclear translocation of TFEB. (e) mRNA expression of TFEB target genes in control and MTMR4-depleted cells. Total RNA was extracted from fed and starved cells and mRNA expression was determined by qPCR. (f) Total cellular LysoTracker-Red fluorescence by flow cytometry analysis in control and MTMR4-depleted cells. A549 cells were transfected with specific siRNAs and FACS analysis. (g) FITC-dextran uptake and degradation assay. After cells uptake FITC-dextran for 1 h, the cells were washed and followed for FITC-dextran remaining in cells for 4 h. The quantified data of FITC dextran remaining in the cells are shown at the right.

FIGURE 6. MTMR4 knockdown inhibits starvation-induced increase in dephosphorylated TFEB/total TFEB ratio.

(a) Phosphorylation of TFEB and other proteins and total amounts of MTMR4 and MTMR3 in control and MTMR4-depleted cells. A549 cells transfected with control- or MTMR4-siRNAs were placed in growth medium (fed) with or without 100 μM chloroquine or in HBSS for 4 h, and subjected to Western blot analyses. S6K, S6 kinase. (b) Quantified data of total TFEB protein level (sum of the dephosphorylated and phosphorylated forms of TFEB) (left), phospho-TFEB level (normalized to GAPDH) (middle) and ratio of dephosphorylated TFEB/total TFEB (right) in control and MTMR4-depleted cells. (c) Time course of starvation-induced change in phosphorylation of TFEB and S6K. A549 cells were starved by culture in HBSS for

the indicated time periods and subjected to Western blot analyses. **Stv**, starved. **(d)** Phosphorylation of TFEB in control and MTMR4–depleted cells under both fed and starved conditions with or without cyclosporine A treatment. Control and MTMR4–depleted A549 cells were incubated in growth medium (fed) or HBSS (starved) with or without cyclosporine-A (10 μ M) for 4 h.

FIGURE 7. MTMR4 knockdown causes accumulation of TFEB in LEs.

(a) Time-lapse imaging of Torin 1 (mTOR inhibitor)–induced TFEB nuclear translocation and its inhibition by MTMR4 knockdown. Torin 1 (1 μ M) was added to A549 cells transfected with the GFP-TFEB expression vector and either control– or MTMR4–specific siRNAs at 1 min. **(b)** Accumulation of GFP-TFEB in LEs but not LYs in MTMR4–depleted cells under the starved condition. GFP-TFEB–transfected cells were placed in growth medium (fed) or HBSS (starved) for 60 min and subjected to immunostaining using anti-LAMP1 (LY marker) and anti-Rab7 (LE marker) antibodies. White arrow heads indicate enrichment of the perinuclear GFP-TFEB signal in Rab7⁺ LEs. White dashed lines indicate nuclear outlines assessed by DAPI staining. Quantified data of colocalization index (Pearson’s correlation coefficient) are shown at the bottom.

FIGURE 8. PI(3)P-phosphatase MTMR4 regulates endocytic and autophagic pathways.

MTMR4 is localized mainly in LEs and APs to regulate PI(3)P levels. MTMR4 regulates the fusion, fission, motility and maturation of endosomes, the autophagic pathway, and lysosomal biogenesis. MTMR4 is also required for activation of TFEB.

This action of MTMR4 contributes to MTMR4 regulation of the endocytic and autophagic pathways.

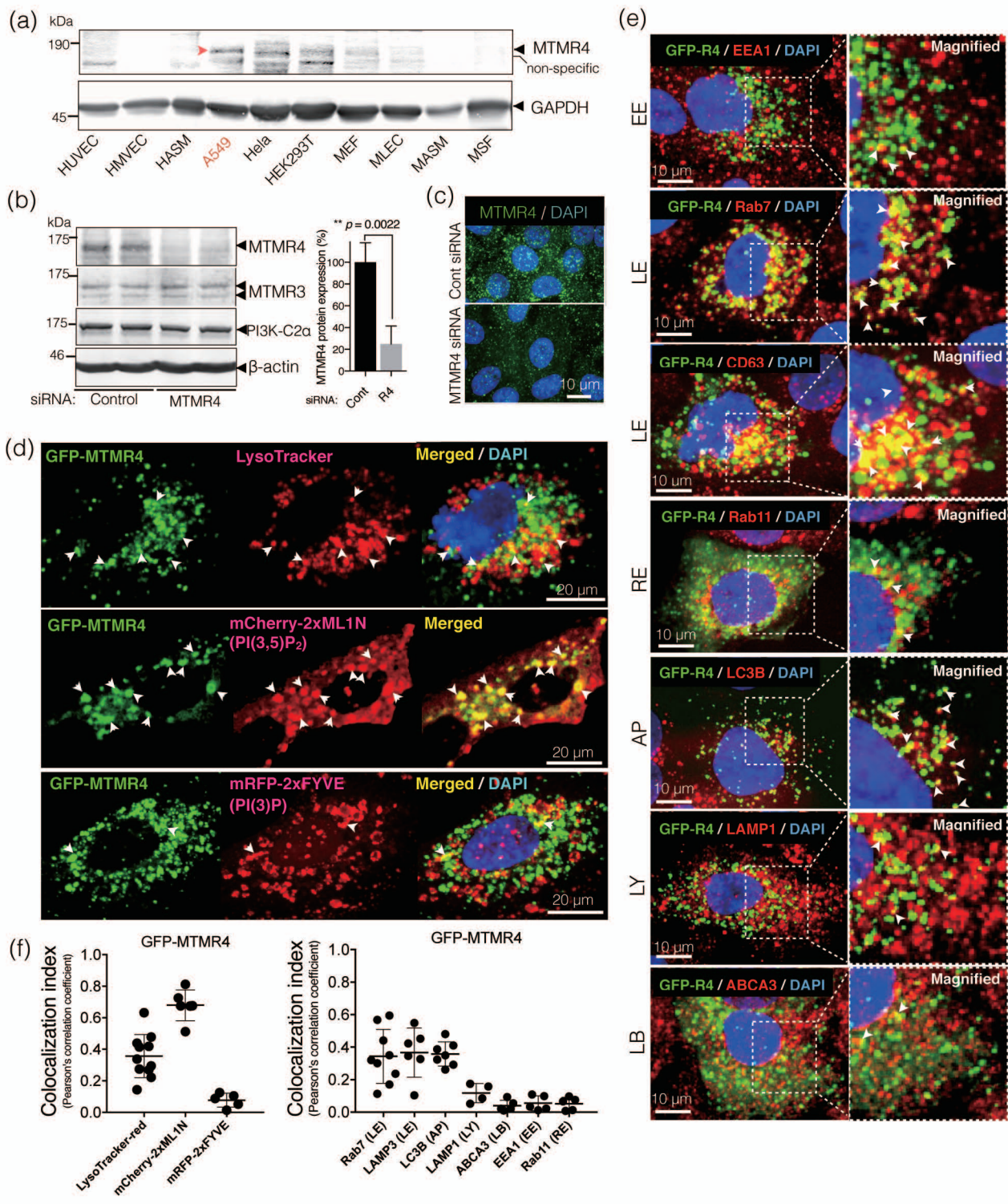


Fig. 1 Hoa *et al.*

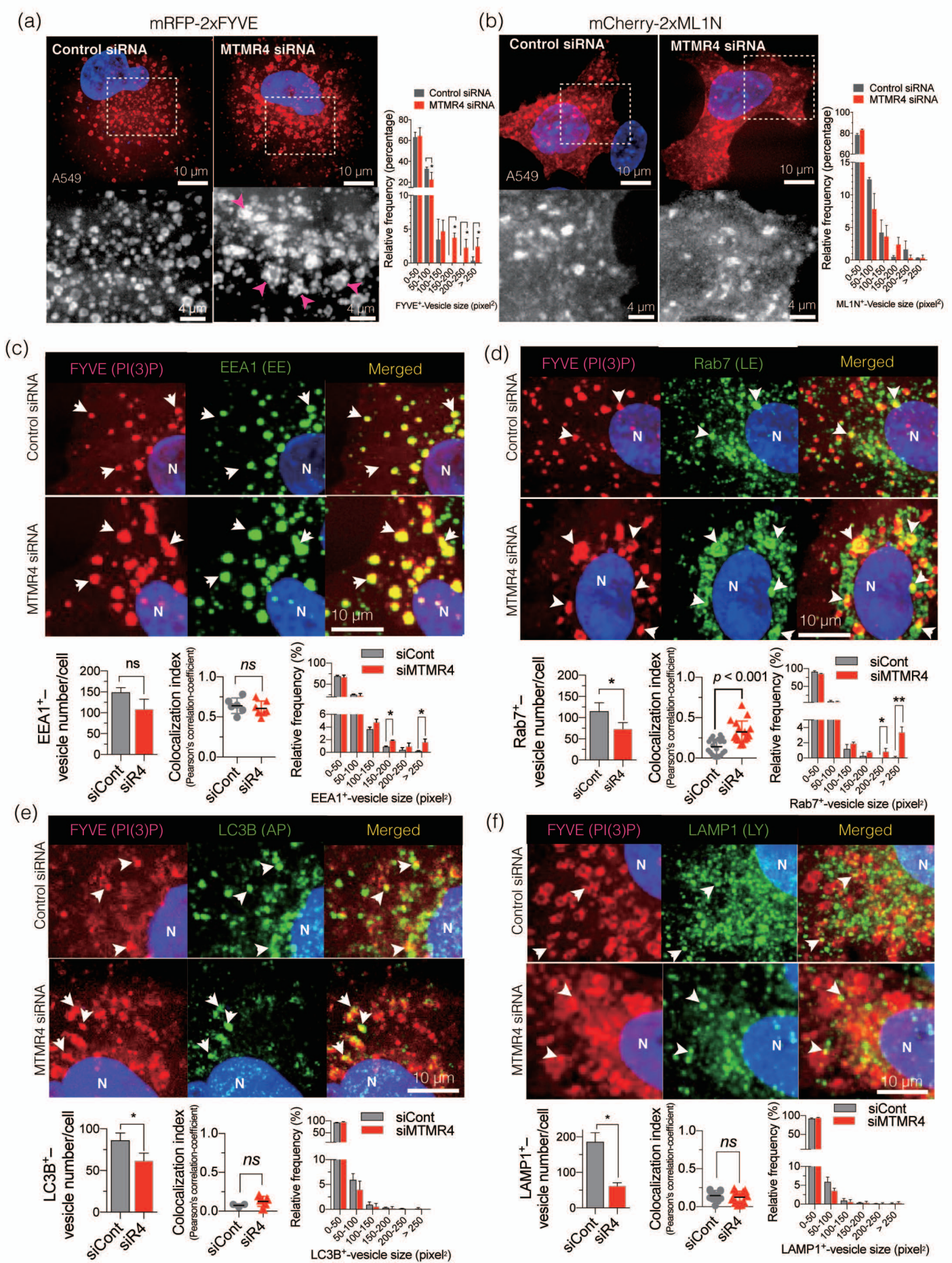


Fig. 2 Hoa *et al.*

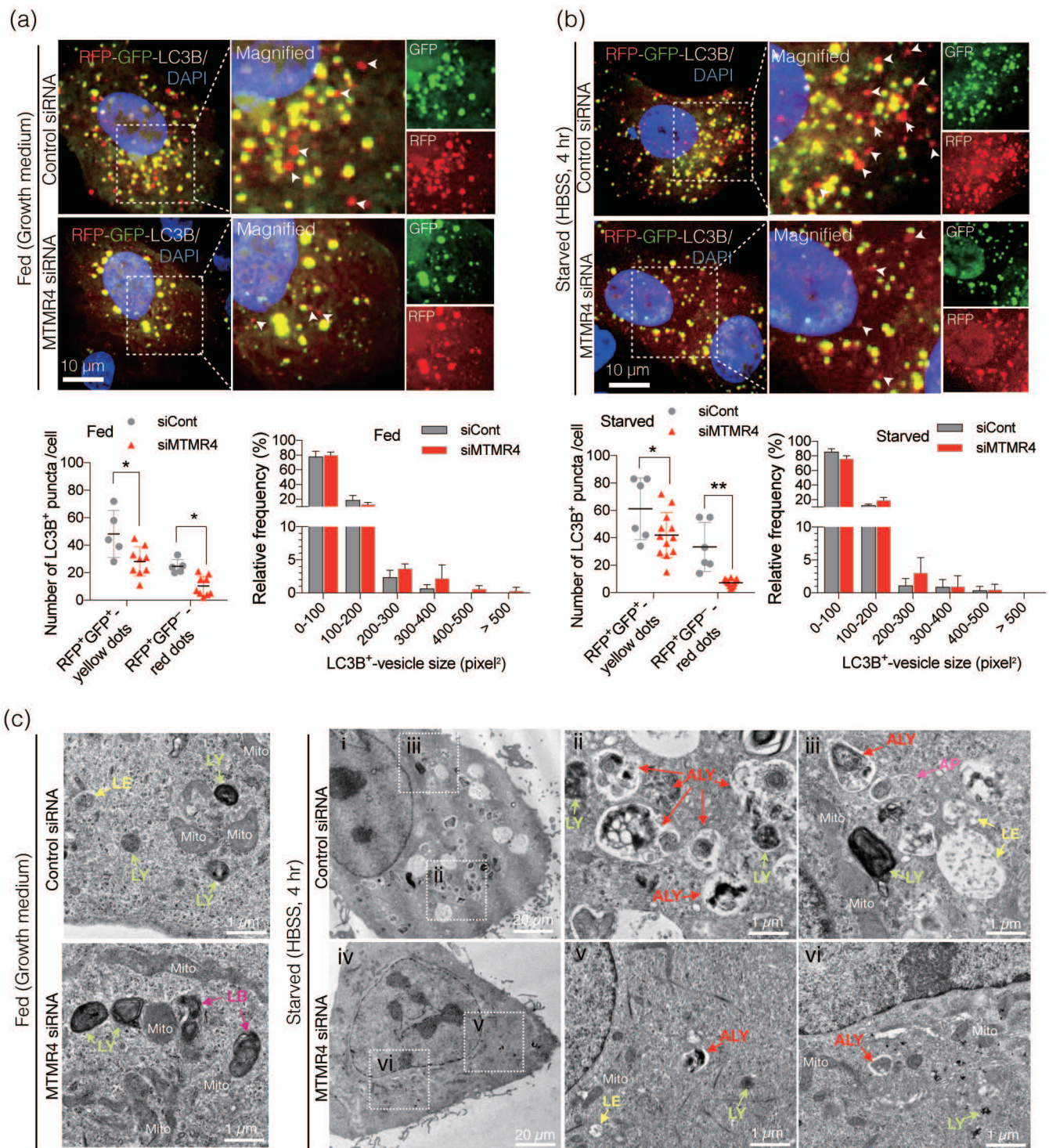


Fig. 3 Hoa *et al.*

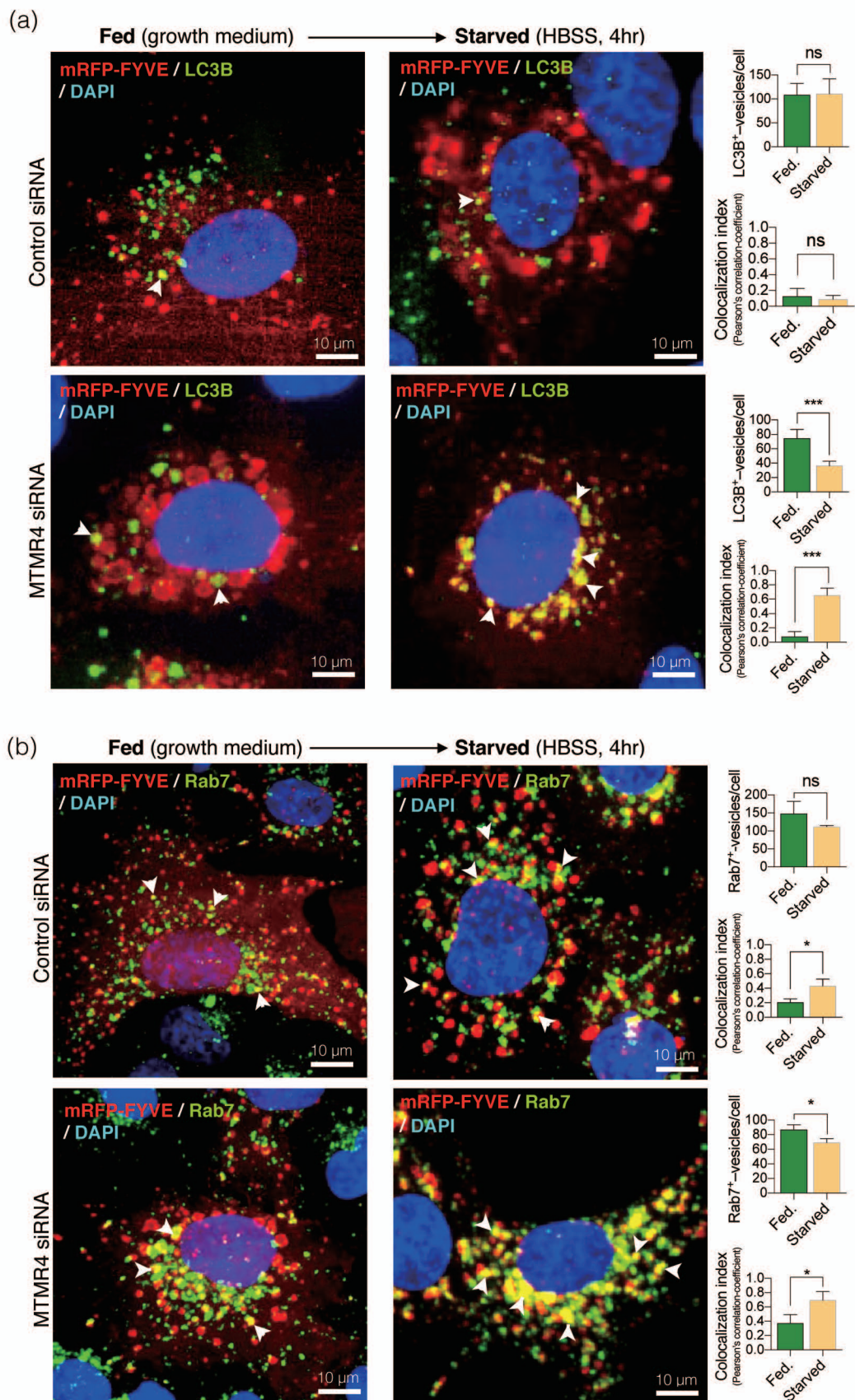


Fig. 4 Hoa *et al.*

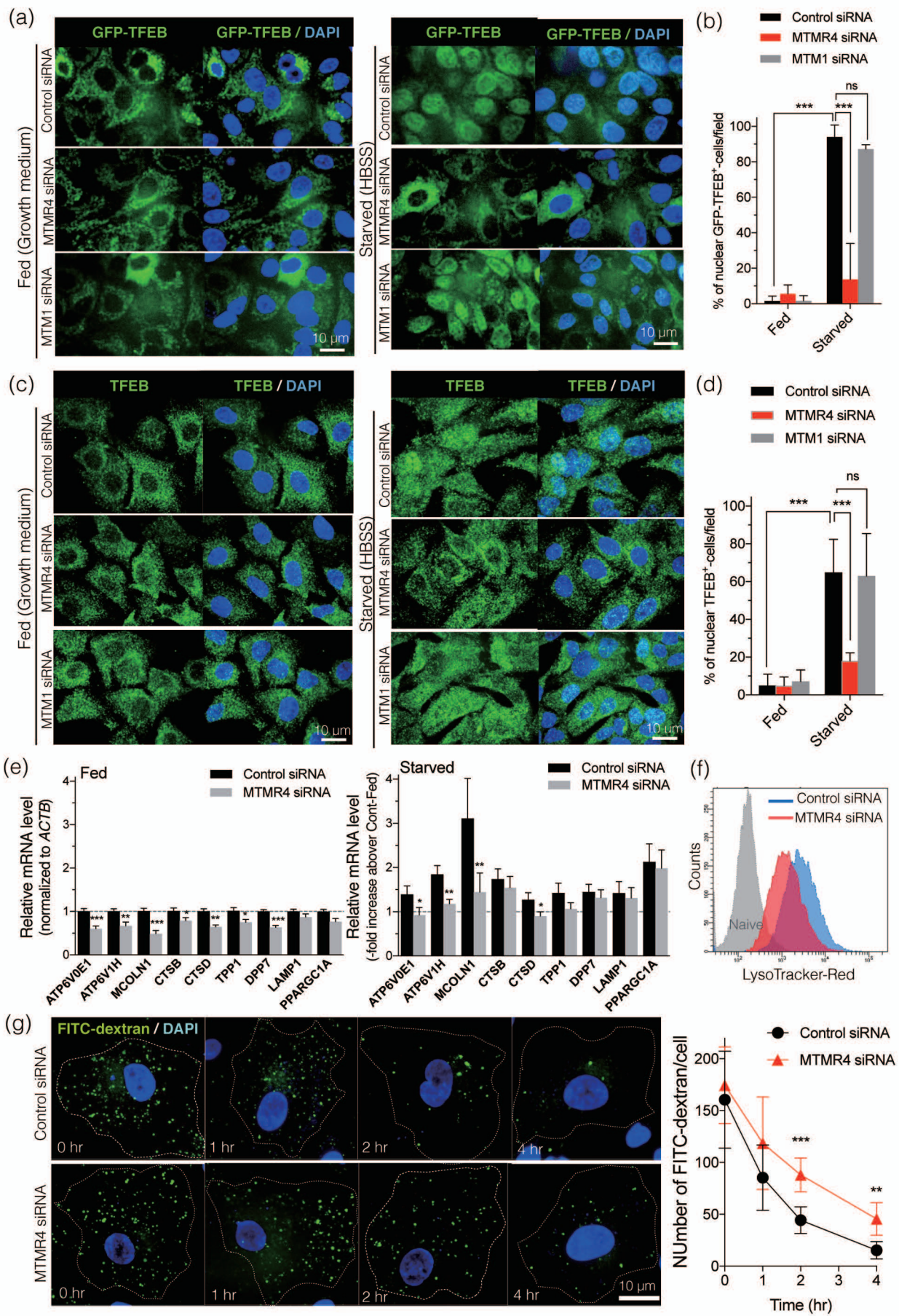


Fig. 5 Hoa *et al.*

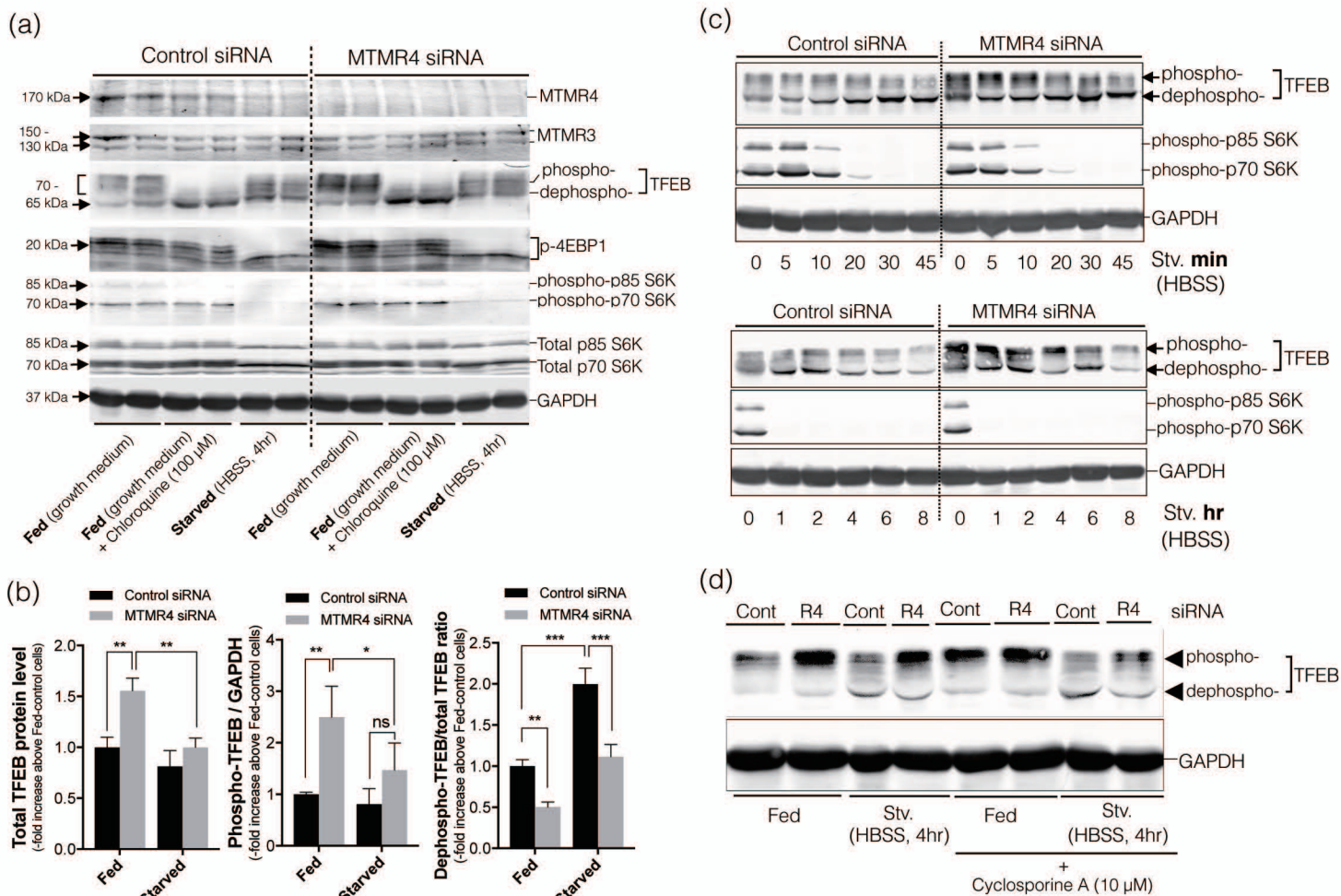


Fig. 6 Hoa *et al.*

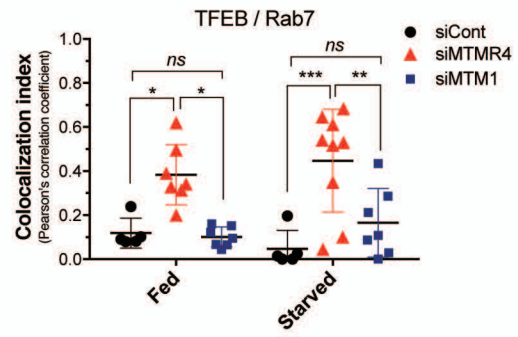
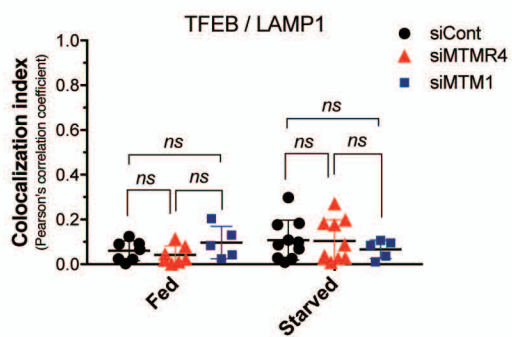
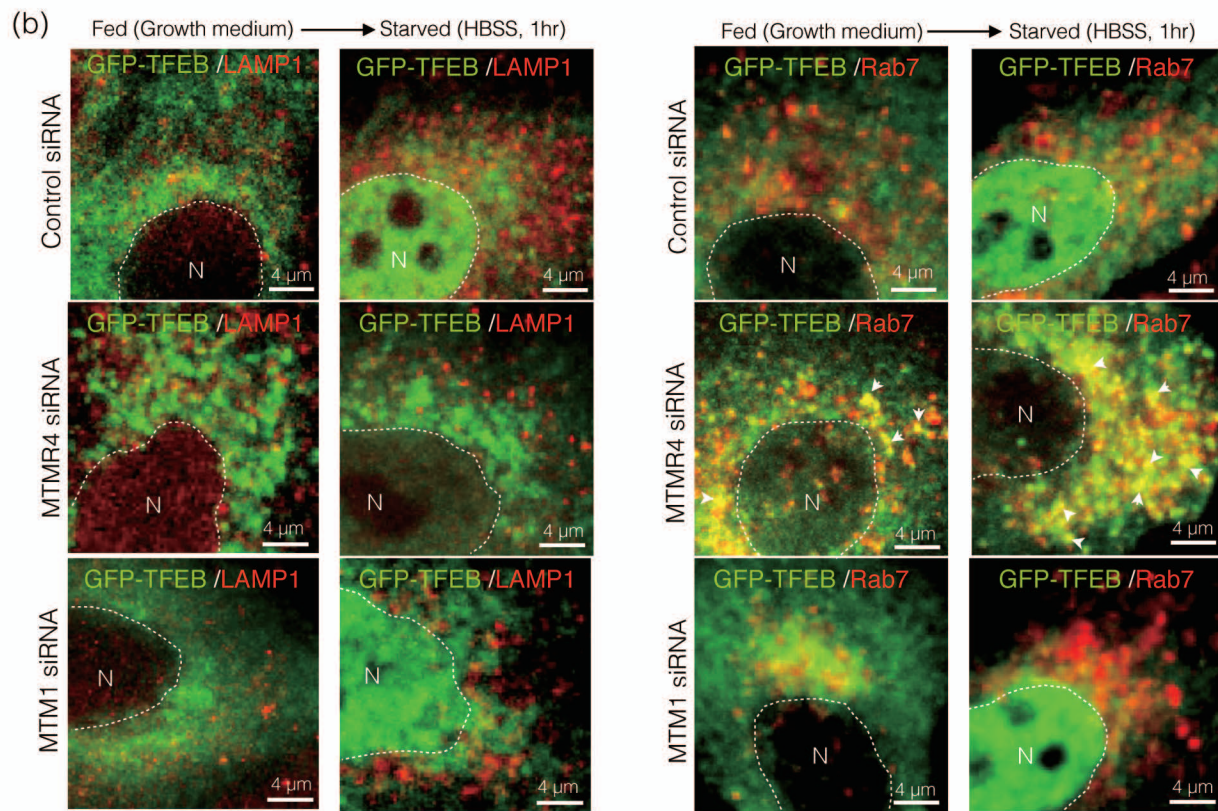
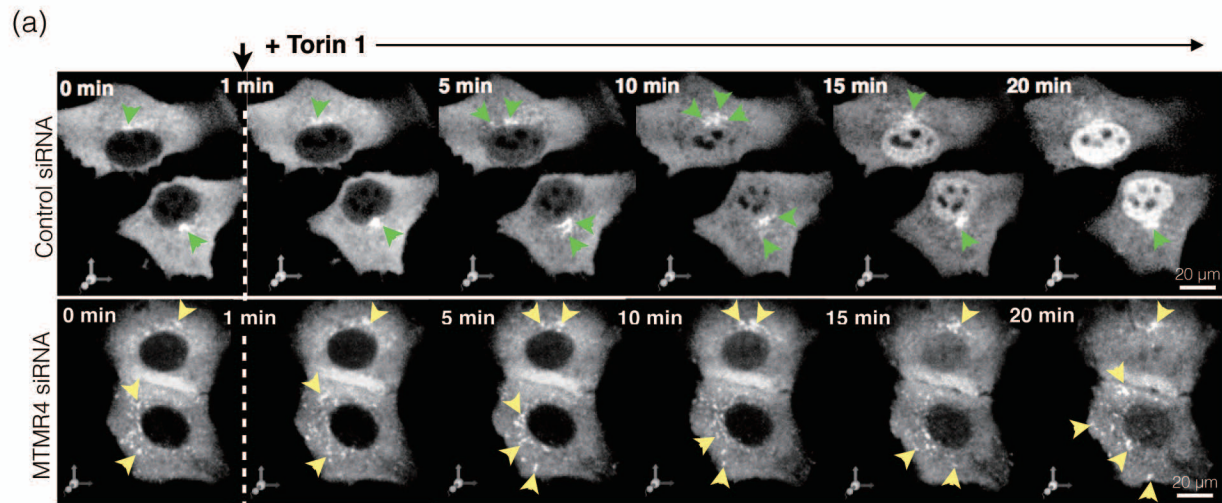


Fig. 7 Hoa *et al.*

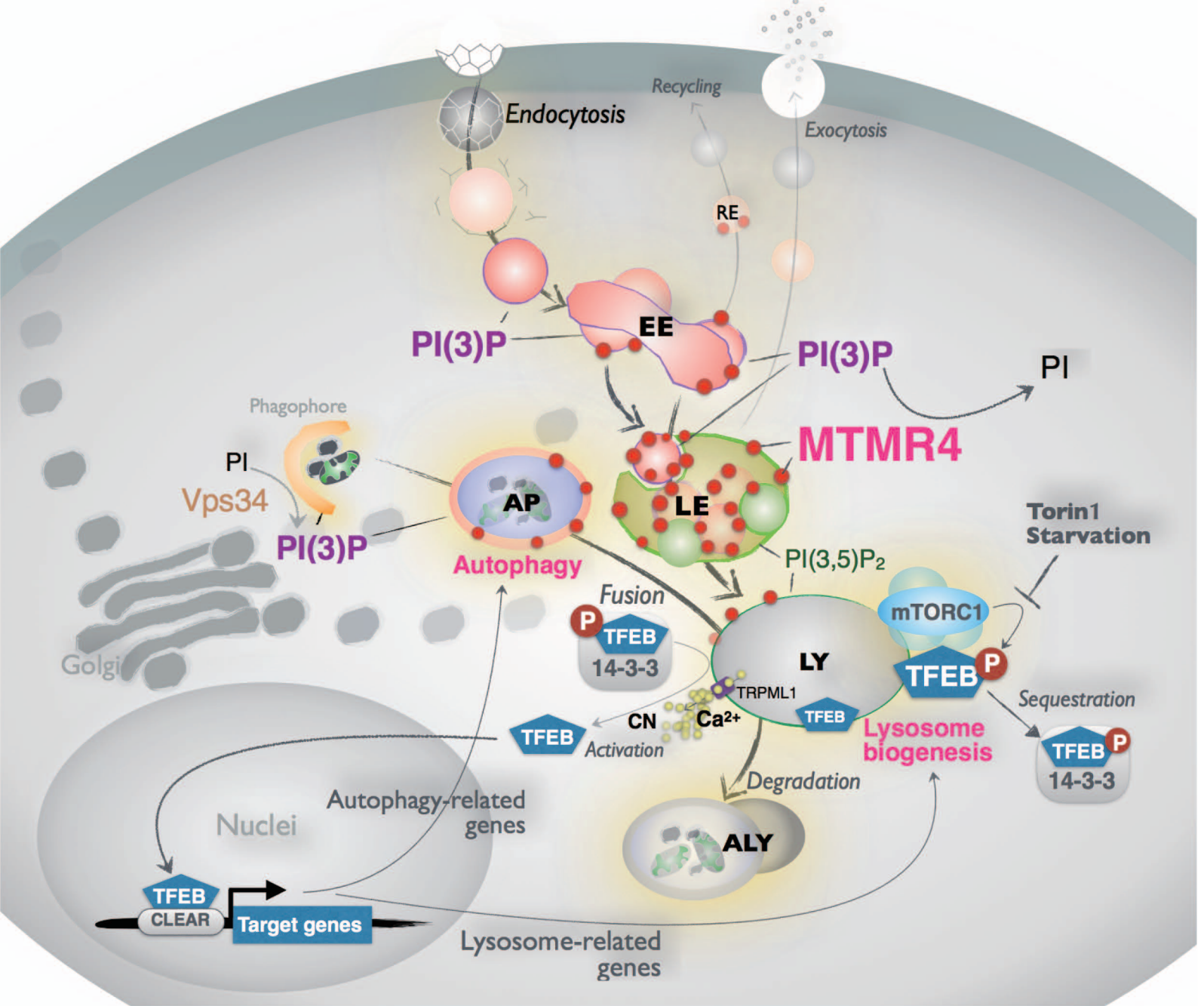


Fig. 8 Hoa *et al.*